Vibrational Analysis of Peptides, Polypeptides, and Proteins. XXIV. Conformation of Poly(α-Aminoisobutyric Acid)

ANIL M. DWIVEDI* and S. KRIMM, *Biophysics Research Division, University of Michigan, Ann Arbor, Michigan 48109*; and B. R. MALCOLM, *Department of Molecular Biology, University of Edinburgh, Edinburgh EH9 3JR, United Kingdom*

Synopsis

Raman and polarized ir spectra have been obtained on built-up monomolecular films of poly(α-aminoisobutyric acid), and analyzed in the context of normal mode calculations on 3_{10}-, α-, and α'-helix conformations of this molecule. The average discrepancy between observed and calculated frequencies is significantly smaller for the 3_{10}-helix than for the other structures. This, together with the more satisfactory explanation of several special features of the spectra, indicates that this polypeptide adopts a 3_{10}-helix conformation in such thin films.

INTRODUCTION

Peptide units containing α-aminoisobutyric acid (AIB) residues exert significant constraints on the conformational freedom of the polypeptide backbone.[1-6] This constraint arises from the steric interactions between the two methyl groups attached to the C^{α} atom, resulting in restrictions on the dihedral angles of the backbone to values very close to those of right- or left-handed 3_{10}-or α-helices.

Burgess and Leach[1] have suggested an obligatory α-helical structure for poly(α-aminoisobutyric acid) (PAIB). Malcolm,[7,8] on the basis of ir and electron-diffraction studies of oriented films of PAIB, has reported a 3_{10}-helical structure. Also, experimental work on small peptides containing AIB residues has demonstrated that the conformation of the backbone is always a right- or left-handed 3_{10}-helix.[9-15] Using classical potential energy functions and energy minimization, Venkataram Prasad and Sasisekharan[2] have worked out the relative stabilities of α- and 3_{10}-helical structures for PAIB. Their analysis indicates the necessity for nonplanar distortion of the peptide units as observed in the crystal structures of peptides with AIB residues,[9-15] and they propose a helical structure with $n = 4$ and $h = 1.5$ Å (named α') as energetically more favorable than the standard 3_{10}-helix. Recently,

* Present address: Analytical Research, Johnson Wax, Racine, WI 53403.

Biopolymers, Vol. 23, 2025-2065 (1984)
 CCC 0006-3525/84/102025-41$04.00

Patterson et al.,[3] in their conformational analysis of oligomers of AIB, have shown that the conformation is very sensitive to the covalent geometry of the residue, particularly the bond angles between the substituents on the C^{α} atom. Symmetrical tetrahedral geometry around C^{α} favors the α-helical conformation, whereas the asymmetric geometry observed in most of the crystals[9-15] gives the 3_{10}-conformation as the favored structure.

Such variations among the various theoretically proposed structures prompted us to undertake a vibrational spectroscopic analysis of the structure of PAIB. With our success in deriving maximally transferrable vibrational force fields for polypeptides,[16-22] we are now in a position to exploit the full potential of vibrational spectroscopy in determining structure in polypeptides and proteins.[23] The applicability of such techniques has already been demonstrated by some of the work reported from our laboratory.[24-30]

Except for brief reports by Elliot[31] and Malcolm,[7] there has been no attempt to analyze the ir and Raman spectra of PAIB. In this paper we report Raman and polarized ir spectra of multimonomolecular layers of PAIB and N-deuterated PAIB (PAIB-ND). Normal mode analysis was carried out using three structural models, the α-helix,[32] the 3_{10}-helix,[2] and the α'-helix.[2] Since the same force field is used for the three calculations, the results distinctly show the influence of conformation on the vibrational frequencies. A comparison between the theoretical prediction and the experimental results clearly indicates that of the three structures, the 3_{10}-helix gives the best frequency fit. Thus, the vibrational analysis suggests that in such very thin films, PAIB has a 3_{10}-helical conformation.

MATERIALS AND METHODS

The polymer employed in this study was a small specimen prepared by W. E. Hanby of Courtaulds Limited and is the same as used previously.[7] Oriented samples were prepared by first dissolving about 5 mg polymer in 0.5 mL dichloroacetic acid, purified by vacuum distillation. The solution was made up to 5 mL with chloroform (reagent grade, redistilled). Approximately 0.005 mL of the solution was spread on the surface of twice-distilled water in a Langmuir trough, forming a molecular monolayer that was then collapsed between two barriers moved across the surface. The final separation of the barriers was slightly greater than the width of the specimen plate used to remove the film. The film was removed by drawing the plate, with an up and down motion, across the surface between the barriers. This produced a specimen oriented with the polymer chains aligned parallel to the up and down motion of the plate. The specimen was dried down on the plate and the procedure was repeated until sufficient polymer had been deposited to give good spectra. Plates of barium fluoride or KRS5

were used for ir spectra and pieces of microscope slide for Raman spectroscopy. N-deuterated specimens were prepared in a similar manner by using O-deuterated dichloroacetic acid, and the monolayers were spread on dilute HCl (pH 3) to minimize exchange with hydrogen.

The ir spectra were recorded on a Perkin-Elmer 577 or 598 spectrophotometer. The peak positions are accurate to $\pm$ 2 cm^{-1}. For polarized ir spectra a wire-grid polarizer with the specimen set at 45° to the slit of the spectrometer was used. Raman spectra were recorded on a Spex 1403 spectrometer at a resolution of ~2 cm^{-1}. The power on the samples, at the 5145-Å line of an Ar ion laser, was about 130 and 100 mW for undeuterated and deuterated specimens, respectively.

NORMAL MODE CALCULATION

Structure, Symmetry, and Selection Rules

For the normal mode calculations we used an isolated helical chain structure, since interchain interactions are expected to be very weak. The structural parameters (bond lengths, bond angles, and hydrogen bonds) and the dihedral angles ($\phi = -57.37°$ and $\psi = -47.49°$) for the α-helical structure were the same as those derived by Arnott and Dover[32] from an x-ray diffraction refinement procedure. For the 3_{10}-helix ($n = 2.99$, $h = 2.01$ Å, $\phi = -45°$, and $\psi = -30°$) and the α'-helix ($n = 4.00$, $h = 1.48$ Å, $\phi = -55°$, and $\psi = -60°$), the structural parameters reported by Venkataram Prasad and Sasisekharan[2] were used. (We have chosen the structure for the 3_{10}-helix that is closest to the standard one, namely, with three residues per turn and an axial repeat of 6 Å.[33] Although it appears not to be the lowest energy structure, the dihedral angles of the latter, viz., $\phi = -50°$, $\psi = -30°$,[2] are close enough that the vibrational frequencies are not expected to be significantly different.) The hydrogen-bonding pattern is different in the three structures, the 3_{10}-helix being of the $i + 3 \rightarrow i$ type, while the α- and α'-helices are of the $i + 4 \rightarrow i$ type. The hydrogen-bond strengths are in the order $3_{10} > \alpha > \alpha'$ (hydrogen-bond parameters for all the three helices are listed in Table I).

Except for H^{α} being replaced by a CH_3 group [the $CH_3(2)$ group], the chemical residue in PAIB is the same as in poly(L-alanine), and thus,

TABLE I
Hydrogen-Bond Parameters for 3_{10}-, α-, and α'-Helices

		3_{10}-Helix	α-Helix	α'-Helix
r(H · · · O)	(Å)	1.828	1.882	2.084
r(N · · · O)	(Å)	2.825	2.857	3.065
< (NHO)	(deg)	175.11	164.19	166.30
< (HNO)	(deg)	3.15	10.34	9.27

for normal mode calculation purposes, the repeat unit has 13 atoms and 49 internal coordinates compared to 10 atoms and 39 internal coordinates in α-poly(L-alanine).[21] The optically active modes are classified into A($\delta = 0°$), E_1($\delta = \theta$), and E_2($\delta = 2\theta$) symmetry species, where δ is the phase difference between the motions in adjacent residues and θ is the angle of rotation per chemical residue about the helical axis; the value of θ is 120°, 99.57°, and 90° for 3_{10}, α, and α′, respectively. Since $\theta = 120°$ for the 3_{10}-helix, the E_1 and E_2 species are degenerate and therefore we report only A and E_1 modes for this structure. The number of modes in each symmetry species and their optical activity for each structure are as follows: 3_{10}: A(Raman, $ir_\parallel$)—37, E_1(Raman, $ir_\perp$)—38; α: A(Raman, $ir_\parallel$)—37, E_1(Raman, $ir_\perp$)—38, E_2(Raman)—39; and α′: A(Raman, $ir_\parallel$)—37, E_1(Raman, $ir_\perp$)—38, E_2(Raman)—39.

Force Field

As a starting point, we transferred without change all the necessary force constants from α-poly(L-alanine),[21] even though we recognized that the presence in PAIB of a CH_3 group in place of H^α would result in different interactions around C^α. This force field was used to compute the frequencies and their potential energy distributions (PED) for the three structural models.

In general, the fit to the experimental data was very satisfactory, with only those modes having the larger contribution from the CH_3 (2) group showing some discrepancies. Besides such discrepancies common to all the structures, a detailed comparison showed that the computed frequencies for the 3_{10}-helix were generally in better agreement with the observed values. For instance, the amide V mode observed at 694 ($ir_\perp$) and 680 ($ir_\parallel$) was predicted at 699 (E_1) and 672 (A) by the 3_{10}-helix, at 656 (E_1) and 629 (A) by the α-helix, and at 625 (E_1) and 619 (A) cm^{-1} by α′-helix. A mixed mode (CN stretch + CC_2 asymmetric stretch + CH_3 rock) observed at 1214 (R) and 1210 ($ir_\parallel$) was predicted at 1194 (A), 1177 (A), and 1186 (A) cm^{-1} by the 3_{10}-, α-, and α′-helices, respectively. Apart from these prominent differences, there were about 10 more cases in which, although the differences were not as large, the 3_{10}-helix gave better agreement. We therefore used the 3_{10}-helix in making slight adjustments in the force constants that influence the CC_2 [$C^\alpha(CH_3)_2$] group (these changes are essentially independent of conformation).

A total of 25 force constants (Table II) required alteration. Of these, the changes in five force constants, namely, *f*(CO), *f*(NH), *f*(H · · · O), *f*(CO ob), and *f*(NH · · · O t), reflect differences in hydrogen-bond geometry and strength between the 3_{10}- and α-helices. The final values of these constants were obtained by manual adjustment. For example, the unperturbed amide A (ν_A^0) mode for PAIB is at ~3260 cm^{-1} (see Results and Discussion), which happens to be the mean of ν_A^0 values

TABLE II
Modified Force Constants Appropriate to Poly(α-Aminoisobutyric Acid)

Force Constant	Value
f(CO)	9.955
f(NH)	5.752
f(H · · · O)	0.135
f(CO ob)	0.687
f(NH · · · O t)	0.0003
$f(C^{\beta}C^{\alpha}C^{\beta})$	1.181
$f(C^{\alpha}C^{\beta}$ t)	0.090
$f(C^{\alpha}C,C^{\alpha}C^{\beta})$	0.301
$f(C^{\alpha}C^{\beta},C^{\alpha}C^{\beta})$	0.100
$f(NC^{\alpha},C^{\beta}C^{\alpha}C^{\beta})$	0.200
$f(C^{\alpha}C,NC^{\alpha}C^{\beta})$	0.100
$f(C^{\alpha}C^{\beta}(1),NC^{\alpha}C^{\beta}(2))$	0.030
$f(C^{\alpha}C^{\beta}(1),CC^{\alpha}C^{\beta}(2))$	0.030
$f(C^{\alpha}C^{\beta},C^{\beta}C^{\alpha}C^{\beta})$	0.517
$f(C^{\alpha}C^{\beta},C^{\alpha}C^{\beta}H)$	0.403
$f(C^{\alpha}CO,CC^{\alpha}C^{\beta})$	0.200
$f(CNC^{\alpha},NC^{\alpha}C^{\beta})$	0.100
$f(C^{\alpha}NH,NC^{\alpha}C^{\beta})$	0.050
$f(NC^{\alpha}C,NC^{\alpha}C^{\beta})$	0.100
$f(NC^{\alpha}C^{\beta},C^{\beta}C^{\alpha}C^{\beta}$	−0.031
$f(NC^{\alpha}C^{\beta},$NH ob)	0.060
$f(CC^{\alpha}C^{\beta},CC^{\alpha}C^{\beta})$	0.100
$f(CC^{\alpha}C^{\beta},C^{\beta}C^{\alpha}C^{\beta})$	−0.031
$f(C^{\beta}C^{\alpha}C^{\beta},C^{\alpha}C^{\beta}H)_T$	0.100
$f(C^{\beta}C^{\alpha}C^{\beta},C^{\alpha}C^{\beta}H)_G$	0.010

for α- and β-poly(L-alanine).[34] This indicates that the hydrogen-bond strength in PAIB is intermediate between those for the α- and β-structures, which is also supported by the structural data [r(N · · · O) for the β-structure is 2.731 Å[20]]. We therefore took for the values of f(CO), f(NH), and f(H · · · O) the mean of the corresponding values for the α- helical[21] and β-sheet[20] structures. The remaining force constants in Table II are associated with the CC_2 group and were refined by a least-squares method. Dispersions in these force constants in the range of 0.1–0.6 average 5%. It is interesting that the force constants associated with the backbone of the chain did not require any alteration, confirming the fact that the conformations of α- and 3_{10}-helices are very close.[4] Although the above force constants were refined for the 3_{10}-helix, they also improved the fit between theoretical and experimental values when used for α and α′ in the final calculations. For a complete force field for PAIB, readers will require all the relevant force constants from our work,[20,21] as well as the 25 constants listed in Table II of this paper. This force field has been used to compute the frequencies of the 3_{10}, α-, and α′-helical structural models for PAIB and the corresponding N-deuterated derivatives.

It should be noted that, as in our earlier work,[18,21] transition dipole

coupling interactions were used to calculate the splittings in amide I and II modes. In the 3_{10}-helix, contributions to the A and E_1 species for amide I are -2.3 and -3.3 cm^{-1}, respectively, and for amide II, -6.6 and 5.9 cm^{-1}, respectively. In the α-helix, contributions to A, E_1, and E_2 species for amide I are -5.5, -7.2, and -16.8 cm^{-1}, respectively, and for amide II, -9.6, 6.2, and 4.2 cm^{-1}, respectively. For the α'-helix such contributions are -0.8, -1.3, and -19.2 cm^{-1}, and -8.4, 4.6, and 6.0 cm^{-1}, respectively. Since the transition dipole parameters are the same, these variations result from the conformational differences between the three structures. The detailed results are discussed in the following section.

RESULTS AND DISCUSSION

Poly(α-Aminoisobutyric Acid)

We present in Fig. 1 the polarized ir spectra of PAIB and PAIB-ND, and in Fig. 2 the Raman spectra of these materials—in both cases,

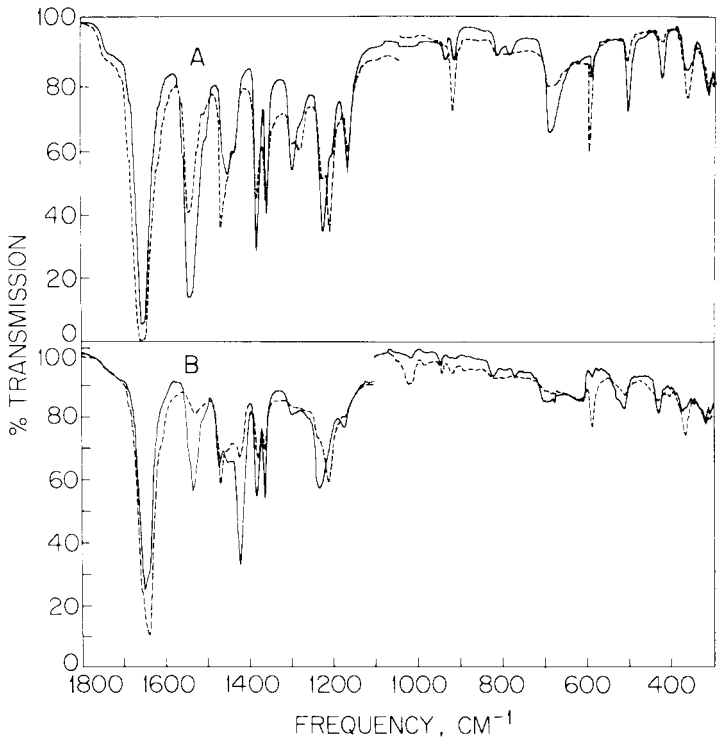

Fig. 1. Polarized ir spectra of (A) poly(α-aminoisobutyric acid) and (B) poly(α-aminoisobutyric acid-ND): Electric vector perpendicular to orientation direction (—) and electric vector parallel to orientation direction (- - -).

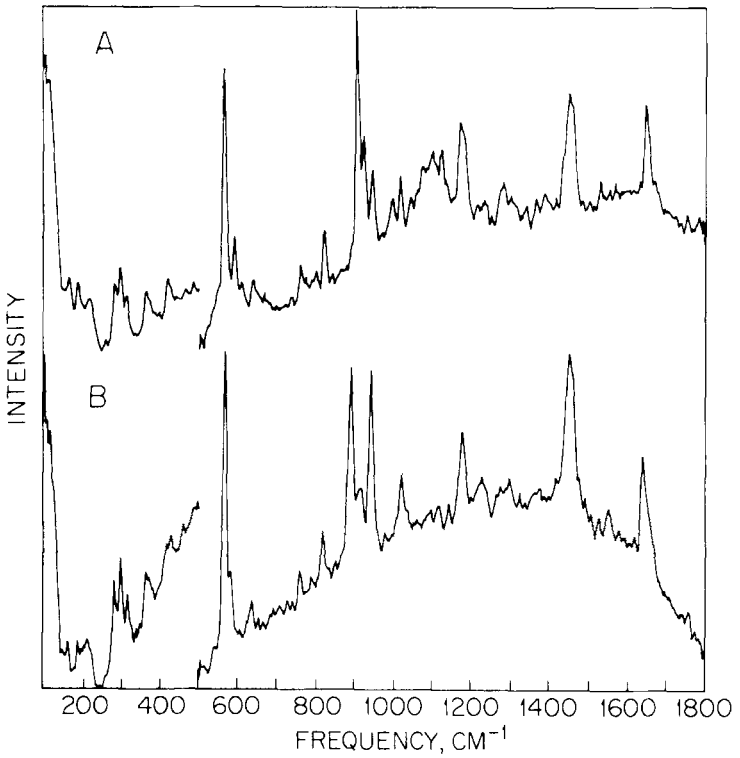

Fig. 2. Raman spectra of (A) poly(α-aminoisobutyric acid) and (B) poly(α-aminoisobutyric acid-ND).

thin films prepared by the Langmuir trough technique described above. The observed band frequencies are given in Tables III and IV, together with the calculated frequencies and PEDs of the 3_{10}-, α-, and α′-helices.

The NH stretch (amide A) mode is observed at 3272 ($ir_{\parallel}$) cm^{-1}. This is lower than the values found for α-poly(L-alanine)[18] (3307 cm^{-1}) and β-poly(L-alanine)[34] (3276 cm^{-1}), which might suggest that the hydrogen bond in PAIB is stronger than those in the other two structures. However, amide A is perturbed by Fermi resonance,[16,34] and therefore, a meaningful conclusion can be drawn only by comparing unperturbed frequencies. The ir spectrum indicates the presence of two amide B modes (of A species, as in the case of amide A), at 3060 and 3030 cm^{-1}. (It might be noted that this is in contrast to the α-helix of poly(L-alanine), which exhibits only a single amide B mode at 3058 cm^{-1}.[34]) The integrated area ratios of these bands to the amide A band are 0.0518 and 0.0566, respectively, leading[16,34] to unperturbed frequencies of ν_A^0 = 3262 cm^{-1}, ν_B^0 = 3070 cm^{-1} and ν_A^0 = 3259 cm^{-1}, ν_B^0 = 3043 cm^{-1}, respectively.

These results lead to some interesting conclusions. The value of

TABLE III
Observed and Calculated Frequencies (in cm $^{-1}$) of Poly(α-Aminoisobutyric Acid)

Observed[a]		Calculated[b]			
Raman	IR	A	E_1	E_2	Potential Energy Distribution[c]
	3260S$_{\parallel}$[d]	3263			NH s(97)
		3261			NH s(98)
		3262			NH s(98)
			3263		NH s(97)
			3261		NH s(98)
			3262		NH s(98)
				3261	NH s(98)
				3262	NH s(98)
2989S	2985S$_{\parallel}$	2986			CH_3(1) as2(49),CH_3(2) as1(35),CH_3(2) as2(14)
		2985			CH_3(2) as1(46),CH_3(1) as2(46)
		2986			CH_3(1) as2(50),CH_3(2) as1(35),CH_3(2) as2(14)
2998M,sh	2995M,sh$_{\perp}$		2986		CH_3(1) as2(50),CH_3(2) as1(35),CH_3(2) as2(14)
			2985		CH_3(2) as1(47),CH_3(1) as2(45)
			2986		CH_3(1) as2(50),CH_3(2) as1(35),CH_3(2) as2(14)
				2985	CH_3(2) as1(47),CH_3(1) as2(45)
				2986	CH_3(1) as2(50),CH_3(2) as1(35),CH_3(2) as2(14)
2989S	2985S$_{\parallel}$	2984			CH_3(1) as1(50),CH_3(2) as2(35),CH_3(2) as1(14)
		2984			CH_3(2) as2(48),CH_3(1) as1(45)
		2984			CH_3(1) as1(51),CH_3(2) as2(34),CH_3(2) as1(14)

2998M,sh	2995M,sh$_\perp$		2984		CH_3(1) as1(52),CH_3(2) as2(33),CH_3(2) as1(14)
			2984		CH_3(1) as1(48),CH_3(2) as2(45)
			2984		CH_3(1) as1(52),CH_3(2) as2(34),CH_3(2) as1(14)
				2984	CH_3(1) as1(46),CH_3(2) as2(46)
				2984	CH_3(1) as1(50),CH_3(2) as2(35),CH_3(2) as1(14)
2989S	2985S$_\parallel$	2984			CH_3(1) as1(49),CH_3(2) as2(38),CH_3(2) as1(12)
		2984			CH_3(1) as1(50),CH_3(2) as2(31),CH_3(2) as1(18)
		2984			CH_3(1) as1(48),CH_3(2) as2(40),CH_3(2) as1(12)
2998M,sh	2995M,sh$_\perp$		2984		CH_3(1) as1(47),CH_3(2) as2(40),CH_3(2) as1(12)
			2984		CH_3(1) as1(46),CH_3(2) as2(33),CH_3(2) as1(19)
			2984		CH_3(1) as1(47),CH_3(2) as2(40),CH_3(2) as1(12)
				2984	CH_3(1) as1(47),CH_3(2) as2(33),CH_3(2) as1(19)
				2984	CH_3(1) as1(49),CH_3(2) as2(39),CH_3(2) as1(12)
2989S	2985S$_\parallel$	2982			CH_3(1) as2(50),CH_3(2) as1(38),CH_3(2) as2(12)
		2982			CH_3(1) as2(49),CH_3(2) as1(32),CH_3(2) as2(18)
		2982			CH_3(1) as2(50),CH_3(2) as1(38),CH_3(2) as2(12)
2998M,sh	2995M,sh$_\perp$		2982		CH_3(1) as2(49),CH_3(2) as1(39),CH_3(2) as2(11)
			2982		CH_3(1) as2(49),CH_3(2) as1(31),CH_3(2) as2(19)
			2982		CH_3(1) as2(49),CH_3(2) as1(38),CH_3(2) as2(12)
				2982	CH_3(1) as2(49),CH_3(2) as1(31),CH_3(2) as2(18)
				2982	CH_3(1) as2(50),CH_3(2) as1(38),CH_3(2) as2(11)

(*continued*)

Table III (*continued*)

Observed[a]		Calculated[b]			
Raman	IR	A	E_1	E_2	Potential Energy Distribution[c]
		2929			$CH_3(2)$ ss(57),$CH_3(1)$ ss(43)
		2929			$CH_3(1)$ ss(74),$CH_3(2)$ ss(25)
		2929			$CH_3(2)$ ss(55),$CH_3(1)$ ss(45)
			2929		$CH_3(1)$ ss(73),$CH_3(2)$ ss(27)
			2929		$CH_3(2)$ ss(53),$CH_3(1)$ ss(46)
			2929		$CH_3(2)$ ss(86),$CH_3(1)$ ss(13)
				2929	$CH_3(2)$ ss(52),$CH_3(1)$ ss(48)
				2929	$CH_3(2)$ ss(70),$CH_3(1)$ ss(30)
2944VS					
2933M,sh	$2935M_1$	2929			$CH_3(1)$ ss(57),$CH_3(2)$ ss(43)
		2929			$CH_3(2)$ ss(74),$CH_3(1)$ ss(25)
		2929			$CH_3(1)$ ss(55),$CH_3(2)$ ss(45)
			2929		$CH_3(2)$ ss(73),$CH_3(1)$ ss(27)
			2929		$CH_3(1)$ ss(53),$CH_3(2)$ ss(46)
			2929		$CH_3(1)$ ss(86),$CH_3(2)$ ss(13)
				2929	$CH_3(2)$ ss(52),$CH_3(1)$ ss(48)
				2929	$CH_3(1)$ ss(70),$CH_3(2)$ ss(30)
	$1656VS_1$	1665			CO s(79),CN s(13),$C^{\alpha}CN$ d(10)
		1657			CO s(81),CN s(12),$C^{\alpha}CN$ d(10)
		1665			CO s(81),CN s(15)

1647S			1661		CO s(81),CN s(13),C^{α}CN d(10)
			1655		CO s(81),CN s(12),C^{α}CN d(10)
			1665		CO s(81),CN s(14),C^{α}CN d(10)
				1646	CO s(81),CN s(12),C^{α}CN d(10)
				1648	CO s(81),CN s(14),C^{α}CN d(10)
	1545VS$_{\perp}$		1547		NH ib(47),CN s(29),C^{α}C s(11),CO ib(11)
			1535		NH ib(41),CN s(32),C^{α}C s(13),CO ib(13)
			1536		NH ib(44),CN s(29),C^{α}C s(12),CO ib(12)
1531W		1533			NH ib(48),CN s(30),CO ib(11),C^{α}C s(10)
		1514			NH ib(42),CN s(34),CO ib(13),C^{α}C s(12)
		1515			NH ib(45),CN s(30),CO ib(12),C^{α}C s(12)
				1538	NH ib(41),CN s(31),C^{α}C s(13),CO ib(13)
				1546	NH ib(43),CN s(27),C^{α}C s(13),CO ib(12)
	1455S$_{\perp}$		1457		CH_3(1) ab1(37),CH_3(2) ab2(30),CH_3(2) ab1(12)
			1457		CH_3(1) ab1(38),CH_3(2) ab2(24),CH_3(2) ab1(18)
			1457		CH_3(1) ab1(37),CH_3(2) ab2(23),CH_3(2) ab1(21)
1457M,sh	1467S$_{\parallel}$	1456			CH_3(1) ab1(40),CH_3(2) ab2(36)
		1456			CH_3(1) ab1(43),CH_3(2) ab2(32)
		1456			CH_3(1) ab1(43),CH_3(2) ab2(31)
				1458	CH_3(1) ab1(36),CH_3(2) ab1(22),CH_3(2) ab2(22)
				1457	CH_3(1) ab1(33),CH_3(2) ab1(24),CH_3(2) ab2(23)
			1454		CH_3(1) ab2(51),CH_3(2) ab1(24)
			1453		CH_3(1) ab2(54),CH_3(2) ab1(18),CH_3(2) ab2(11)
			1454		CH_3(1) ab2(52),CH_3(2) ab1(19),CH_3(2) ab2(12)

(*continued*)

Table III (*continued*)

Observed[a]		Calculated[b]			
Raman	IR	A	E_1	E_2	Potential Energy Distribution[c]
1450S		1452			CH_3(2) ab1(45),CH_3(1) ab2(29)
		1452			CH_3(2) ab1(45),CH_3(1) ab2(23),CH_3(2) ab2(15)
		1453			CH_3(2) ab1(48),CH_3(1) ab2(23),CH_3(2) ab2(13)
				1454	CH_3(1) ab2(64),CH_3(2) ab1(10),CH_3(2) ab2(10)
				1454	CH_3(1) ab2(64),CH_3(2) ab1(11)
1450S		1450			CH_3(1) ab2(41),CH_3(2) ab1(34),CH_3(1) ab1(13)
		1450			CH_3(1) ab2(41),CH_3(2) ab1(30),CH_3(1) ab1(16)
		1451			CH_3(1) ab2(51),CH_3(2) ab1(25),CH_3(1) ab1(10)
			1450		CH_3(2) ab1(49),CH_3(1) ab2(21),CH_3(1) ab1(16)
			1450		CH_3(2) ab1(44),CH_3(1) ab1(27),CH_3(1) ab2(13)
			1450		CH_3(2) ab1(43),CH_3(1) ab1(22),CH_3(1) ab1(17)
				1450	CH_3(2) ab1(50),CH_3(1) ab1(31)
				1450	CH_3(2) ab1(50),CH_3(1) ab1(22),CH_3(1) ab2(11)
1450S		1449			CH_3(2) ab2(44),CH_3(1) ab1(32),CH_3(1) ab2(14)
		1449			CH_3(2) ab2(41),CH_3(1) ab1(28),CH_3(1) ab2(21)
		1449			CH_3(2) ab2(44),CH_3(1) ab1(33),CH_3(1) ab2(13)
			1449		CH_3(2) ab2(48),CH_3(1) ab1(32),CH_3(1) ab2(10)
			1449		CH_3(2) ab2(48),CH_3(1) ab1(21),CH_3(1) ab2(17)
			1449		CH_3(2) ab2(47),CH_3(1) ab1(32),CH_3(1) ab2(11)
				1449	CH_3(2) ab2(55),CH_3(1) ab1(19),CH_3(1) ab2(13)
				1449	CH_3(2) ab2(51),CH_3(1) ab1(32)

1386W	1385S$_{\perp}$		1387		CH_3(2) sb(46),CH_3(1) sb(28)
			1387		CH_3(2) sb(43),CH_3(1) sb(33)
			1390		CH_3(2) sb(37),CH_3(1) sb(34)
		1386			CH_3(1) sb(48),CH_3(2) sb(35)
		1388			CH_3(1) sb(47),CH_3(2) sb(33)
		1392			CH_3(1) sb(43),CH_3(2) sb(29)
				1387	CH_3(2) sb(48),CH_3(1) sb(23)
				1389	CH_3(2) sb(44),CH_3(1) sb(21)
			1369		CH_3(1) sb(64),CH_3(2) sb(29)
			1366		CH_3(1) sb(57),CH_3(2) sb(44)
			1367		CH_3(1) sb(52),CH_3(2) sb(49)
1364W	1361S$_{\parallel}$	1366			CH_3(2) sb(62),CH_3(1) sb(40)
		1366			CH_3(2) sb(64),CH_3(1) sb(39)
		1366			CH_3(2) sb(66),CH_3(1) sb(35)
				1367	CH_3(1) sb(71),CH_3(2) sb(29)
				1367	CH_3(1) sb(73),CH_3(2) sb(28)
1339W			1346		CH_3(2) sb(21),NH ib(19),NC^{α} s(15),$C^{\alpha}C$ s(11)
			1334		NC^{α} s(20),NH ib(19)
			1334		NH ib(23),NC^{α} s(15)
1313VW		1312			NH ib(22),NC^{α} s(14),CC_2 ss(11),CH_3(1) sb(10)
		1311			NC^{α} s(20),NH ib(16),CC_2 ss(14)
		1316			NH ib(26),CH_3(1) sb(21),CC_2 as(13)
				1345	NH ib(19),NC^{α} s(18),CH_3(2) sb(16)
				1347	CH_3(2) sb(24),NH ib(22),NC^{α} s(14)

(*continued*)

Table III (*continued*)

Observed[a]		Calculated[b]			
Raman	IR	A	E_1	E_2	Potential Energy Distribution[c]
1302W	1304$S_\perp$		1302		CC_2 ss(24),NC^α s(16),$C^\alpha C$ s(11)
			1296		CC_2 ss(19),NH ib(16),$C^\alpha C$ s(15),NC^α s(11)
			1296		CC_2 ss(17),NC^α s(16),$C^\alpha C$ s(12)
1280M	1280$M_\parallel$	1287			$C^\alpha C$ s(24),NC^α s(20),CC_2 w(13),NH ib(10)
		1295			$C^\alpha C$ s(21),NH ib(19),NC^α s(15),CC_2 as(11),CC_2 w(10),CH_3(1) sb(10)
		1300			NC^α s(31),CC_2 w(14),$C^\alpha C$ s(13)
				1293	CC_2 ss(26),NH ib(16),$C^\alpha C$ s(14),NC^α s(10),CH_3(1) rl(10)
				1285	CC_2 ss(26),$C^\alpha C$ s(13),NC^α s(12),CH_3(1) rl(11),NH ib(10)
1230W		1230			CC_2 as(60),CH_3(1) rl(17),CC_2 r(11),CH_3(2) sb(10)
		1228			CC_2 as(50),CH_3(1) rl(17)
		1235			CC_2 as(55),CH_3(1) rl(13),CH_3(2) sb(11),CC_2 r(10)
	1227$S_\perp$		1230		CC_2 as(81),CC_2 r(15)
			1224		CC_2 as(66),CC_2 r(12)
			1233		CC_2 as(64),CC_2 r(11)
				1225	CC_2 as(74),CC_2 r(13)
				1233	CC_2 as(76),CC_2 r(13),CH_3(1) sb(10)
1214W	1210$S_\parallel$	1196			CC_2 as(19),CN s(14),CH_3(2) rl(14)
		1182			CC_2 as(17),CN s(16),CH_3(2) rl(13),NH ib(12)
		1186			CN s(16),CH_3(2) rl(13),CC_2 as(11)
1170S	1170$S_\perp$		1165		CH_3(2) rl(19),CN s(18),CH_3(1) r2(14),CC_2 w(11)
			1166		CN s(18),CH_3(2) rl(16),CH_3(1) r2(12),NH ib(11)
			1168		CN s(18),CH_3(2) rl(16),CH_3(1) r2(11)

				1158	CN s(19),CH_3(2) rl(17),CH_3(1) r2(15),CC_2 w(11),NH ib(10)
				1157	CN s(19),CH_3(2) rl(18),CH_3(1) r2(17),CC_2 w(12)
			1023		CH_3(1) r2(47),CH_3(2) rl(32),CH_3(2) r2(11)
			1023		CH_3(1) r2(47),CH_3(2) rl(32),CH_3(2) r2(11)
			1022		CH_3(1) r2(47),CH_3(2) rl(33),CH_3(2) r2(10)
1018M	1020VW$_{\|}$	1022			CH_3(1) r2(46),CH_3(2) rl(33),CH_3(2) r2(11)
		1023			CH_3(1) r2(46),CH_3(2) rl(33),CH_3(2) r2(10)
		1022			CH_3(1) r2(46),CH_3(2) rl(34),CH_3(2) r2(10)
				1023	CH_3(1) r2(48),CH_3(2) rl(30),CH_3(2) r2(12)
				1023	CH_3(1) r2(47),CH_3(2) rl(31),CH_3(2) r2(11)
			1000		CH_3(1) rl(38),CH_3(2) r2(31),CC_2 as(16)
			997		CH_3(1) rl(36),CH_3(2) r2(31),CC_2 as(16)
			1000		CH_3(1) rl(39),CH_3(2) r2(31),CC_2 as(14)
996MW		999			CH_3(1) rl(39),CH_3(2) r2(28),CC_2 as(17)
		997			CH_3(1) rl(39),CH_3(2) r2(27),CC_2 as(17),CH_3(2) rl(10)
		1000			CH_3(1) rl(41),CH_3(2) r2(28),CC_2 as(14),CH_3(2) rl(10)
				998	CH_3(2) r2(35),CH_3(1) rl(33),CC_2 as(15)
				1000	CH_3(1) rl(35),CH_3(2) r2(35),CC_2 as(14)
			980		CH_3(1) rl(23),CH_3(2) r2(23),CC_2 ss(18),NC^{α} s(13)
			977		CH_3(1) rl(24),CH_3(2) r2(24),CC_2 ss(21),NC^{α} s(13)
			972		CH_3(2) rl(22),CC_2 ss(19),CH_3(1) rl(19),NC^{α} s(14)
950M	953VW$_{\|}$	958			CH_3(2) r2(24),NC^{α} s(21),CC_2 ss(18),CH_3(1) r2(17),CH_3(1) rl(10)
		965			CH_3(2) r2(28),CC_2 ss(22),NC^{α} s(18),CH_3(1) rl(13),CH_3(1) r2(12)
		962			CH_3(2) r2(26),NC^{α} s(20),CH_3(1) r2(17),CC_2 ss(16)

(*continued*)

Table III (*continued*)

Observed[a]		Calculated[b]			
Raman	IR	A	E_1	E_2	Potential Energy Distribution[c]
				984	CH_3(1) rl(30),CH_3(2) r2(22),CC_2 ss(19),NC$^{\alpha}$ s(11)
				979	CH_3(1) rl(28),CH_3(2) r2(21),CC_2 ss(20),NC$^{\alpha}$ s(11)
	940W$_{\perp}$		940		CN s(17),CH_3(2) rl(12),CH_3(1) r2(11),CNC$^{\alpha}$ d(10)
			941		CN s(16),CH_3(2) rl(13),CNC$^{\alpha}$ d(10)
			935		CN s(16),CH_3(2) rl(11)
923M	920S$_{\parallel}$	926			CC_2 ss(33),C$^{\alpha}$C s(20),CH_3(2) rl(13)
		929			CC_2 ss(22),C$^{\alpha}$C s(22),CH_3(2) rl(14),CH_3(1) r2(12)
		929			CC_2 ss(25),C$^{\alpha}$C s(19),CN s(13)
				944	CN s(16),CH_3(2) rl(15),CH_3(1) r2(11),CNC$^{\alpha}$ d(10)
				940	CN s(17),CH_3(2) rl(13),CH_3(1) r2(11),CNC$^{\alpha}$ d(10)
908VS	905VW$_{\parallel}$	905			CNC$^{\alpha}$ d(22),CN s(13),C$^{\alpha}$CN d(11),CO ib(11)
		902			CNC$^{\alpha}$ d(20),CC_2 ss(14),C$^{\alpha}$CN d(11),CN s(11),CO ib(10)
		902			CNC$^{\alpha}$ d(18),CC_2 ss(16),C$^{\alpha}$CN d(10)
823M	820M$_{\perp}$		832		CC_2 ss(42),NC$^{\alpha}$ s(17),CO ib(11)
			849		CC_2 ss(31),NC$^{\alpha}$ s(15),CO ib(10)
			857		CC_2 ss(27),NC$^{\alpha}$ s(16),CO ib(10)
				812	CC_2 ss(54),NC$^{\alpha}$ s(16)
				811	CC_2 ss(54),CO ob(19)
790VW	790MW$_{\perp}$		782		CO ob(49),CN t(13),CC_2 ss(10)
			781		CO ob(48),CC_2 ss(13)
			788		CO ob(46),CC_2 ss(17)

762W		778			CO ob(41),CN t(31)
		767			CO ob(44),CN t(26)
		767			CO ob(46),CN t(22)
				785	CO ob(50)
				796	CO ob(35),NC$^{\alpha}$ s(22)
	694$S_{\perp}$		701		CN t(54),NH ob(30),CO ob(11),NH· · ·O ib(11)
			659		CN t(65),NH ob(35),NH· · ·O ib(12)
			625		CN t(75),NH ob(37)
	680$MW_{\parallel}$	676			NH ob(40),CN t(37),CO ob(27),CC_2 r(13),NH· · ·O ib(10)
		628			CN t(55), NH ob(44),CO ob(23),NH· · ·O ib(11),CC_2 r(11)
		619			CN t(46),NH ob(17)
				688	CN t(27),C$^{\alpha}$C s(18),CC_2 w(14)
				692	C$^{\alpha}$C s(22),CC_2 w(17),CN t(17),CO ib(10)
642W			640		CO ib(18),CC_2 w(18),C$^{\alpha}$C s(17),CN t(11)
			628		CC_2 w(18),CN t(17),CO ib(16),C$^{\alpha}$C s(12)
			619		CO ib(16),CC_2 w(16),C$^{\alpha}$CN d(14),C$^{\alpha}$C s(13)
				654	CN t(61),NH ob(39),NH· · ·O ib(12)
				625	CN t(80),NH ob(NHob)(42)
594M	595$S_{\parallel}$	594			NC$^{\alpha}$C d(16),CC_2 ss(15),CN t(13),NC$^{\alpha}$ s(10),CC_2 b(10)
		593			NC$^{\alpha}$C d(18),CC_2 ss(13),NC$^{\alpha}$ s(10),CC_2 w(10)
		595			NH ob(20),NC$^{\alpha}$C d(17),CO ob(11)
568S		557			C$^{\alpha}$CN d(35),CC_2 w(31),CO ib(21)
		561			C$^{\alpha}$CN d(32),CC_2 w(22),CN t(16),CO ib(15)
		542			CN t(37),CC_2 w(23),NH ob(21),C$^{\alpha}$CN d(21),CO ib(17), CO ob(13)

(*continued*)

Table III (*continued*)

Observed[a]		Calculated[b]			
Raman	IR	A	E_1	E_2	Potential Energy Distribution[c]
506W	$505S_{\perp}$		506		CC_2 r(38),$NC^{\alpha}C$ d(14)
			499		CC_2 r(34),$NC^{\alpha}C$ d(15)
			502		CC_2 r(32),$NC^{\alpha}C$ d(12)
				477	CC_2 r(29),CO ib(14),$NC^{\alpha}C$ d(10),$C^{\alpha}C$ s(10)
				477	CC_2 r(28),CO ib(24),$C^{\alpha}C$ s(11)
		435			CC_2 tw(35),CC_2 b(22),CC_2 r(13)
		425			CC_2 b(32),CC_2 tw(19),CC_2 w(13),CC_2 r(11)
		424			CC_2 b(38),CC_2 tw(17),CC_2 w(11)
422M	$425M_{\perp}$		433		CC_2 b(54),CO ib(14)
			442		CC_2 b(46),CO ib(12)
			456		CC_2 b(37),CO ib(13),NH ob(12),$C^{\alpha}CN$ d(11)
				415	CC_2 b(64)
				424	CC_2 b(47),CC_2 tw(15),$NC^{\alpha}C$ d(13)
367M	$367M_{\perp}$		361		CC_2 w(20),CC_2 tw(18),$C^{\alpha}CN$ d(15),CC_2 b(11),CO ib(10)
			353		CC_2 w(17),CO ib(16),CC_2 tw(16),CC_2 b(11)
			361		CC_2 b(23),CC_2 tw(15),CC_2 w(13)
	$362S_{\parallel}$	351			CC_2 w(32),CC_2 b(16)
		364			CC_2 w(23),CC_2 b(19),CC_2 r(12),CO ob(12)
		366			CC_2 w(33),CC_2 b(15),CO ob(15)
				376	CC_2 tw(36),CC_2 b(17),$C^{\alpha}CN$ d(16),CC_2 r(10)
				387	CC_2 tw(31),CC_2 b(29),$C^{\alpha}CN$ d(14)

		330			CO ib(29),CC_2 r(23),CNC^{α} d(11)
		337			CO ib(38),$C^{\alpha}C$ s(14),CC_2 w(12),CC_2 r(12)
		322			CO ib(36),CC_2 r(16),$C^{\alpha}C$ s(13)
316M	$313M_{\perp}$		324		CC_2 tw(23),CC_2 b(14),CO ib(14),CNC^{α} d(10),$NC^{\alpha}C$ d(10)
			326		CC_2 b(22),CC_2 tw(22),CO ib(12),$NC^{\alpha}C$ d(11)
			317		CO ib(21),CC_2 b(18),CC_2 tw(15),$NC^{\alpha}C$ d(12)
				318	CO ib(18),CC_2 w(17)
				310	CC_2 w(17),CO ib(16),CC_2 r(16)
298S		289			CC_2 b(36),CC_2 tw(30)
		284			CC_2 tw(42),CC_2 b(30)
		280			CC_2 tw(46),CC_2 b(26)
284M			276		CC_2 w(19),CC_2 tw(18),CC_2 r(11),CO ob(11),CC_2 b(10)
			289		CC_2 tw(30),CC_2 w(20),CC_2 b(12),CC_2 r(10)
			289		CC_2 tw(34),CC_2 w(20),CC_2 b(11),CC_2 r(10)
				268	CC_2 w(17),CC_2 tw(17),CO ob(15),$NC^{\alpha}C$ d(12)
				275	CC_2 w(25),$NC^{\alpha}C$ d(13),CC_2 tw(10),CO ob(10)
220M		223			$C^{\alpha}C^{\beta}$ t(94)
		224			$C^{\alpha}C^{\beta}$ t(83)
		222			$C^{\alpha}C^{\beta}$ t(85)
			223		$C^{\alpha}C^{\beta}$ t(93)
			224		$C^{\alpha}C^{\beta}$ t(96)
			224		$C^{\alpha}C^{\beta}$ t(96)
				223	$C^{\alpha}C^{\beta}$ t(89)
				224	$C^{\alpha}C^{\beta}$ t(89)

(*continued*)

Table III (*continued*)

Observed[a]		Calculated[b]			
Raman	IR	A	E_1	E_2	Potential Energy Distribution[c]
220M		220			$C^{\alpha}C^{\beta}$ t(97)
		219			$C^{\alpha}C^{\beta}$ t(98)
		219			$C^{\alpha}C^{\beta}$ t(98)
			218		$C^{\alpha}C^{\beta}$ t(96)
			218		$C^{\alpha}C^{\beta}$ t(98)
			218		$C^{\alpha}C^{\beta}$ t(97)
				219	$C^{\alpha}C^{\beta}$ t(95)
				220	$C^{\alpha}C^{\beta}$ t(96)
189M			188		$C^{\alpha}CN$ d(28),CC_2 tw(11)
			176		$C^{\alpha}CN$ d(30),CC_2 r(11)
			171		$C^{\alpha}CN$ d(23),CC_2 tw(10)
165M		165			$C^{\alpha}CN$ d(22),CC_2 tw(18),NH ob(10)
		187			CC_2 tw(22),$C^{\alpha}CN$ d(17),$C^{\alpha}C^{\beta}$ t(10)
		181			CC_2 tw(19),$C^{\alpha}CN$ d(15),CNC^{α} d(12)
				197	$C^{\alpha}CN$ d(29),CC_2 tw(14),CC_2 w(11),CC_2 r(10)
				194	$C^{\alpha}CN$ d(35),CC_2 tw(20)
		137			CNC^{α} d(38),CC_2 r(16),$C^{\alpha}CN$ d(12),H· · ·O s(10)
		116			CNC^{α} d(39),CC_2 r(25),$C^{\alpha}CN$ d(19)
		112			CNC^{α} d(33),CC_2 r(28),$C^{\alpha}CN$ d(25)
115W			121		CNC^{α} d(30),Nh ob(22)
			131		CNC^{α} d(39),CC_2 r(13),NH ob(12)
			136		CNC^{α} d(29),CC_2 r(21),H· · ·O s(15),$C^{\alpha}CN$ d(12)

			122	CNC^{α} d(31),NH ob(24),CC_2 r(12)
			138	CNC^{α} d(26),CC_2 r(15),H· · ·O s(11),CO ob(10)
		92		H· · ·O s(20),$C^{\alpha}C$ t(17),NH ob(16),NC^{α} t(13),CN t(10)
		88		$C^{\alpha}C$ t(21),NH ob(19),NC^{α} t(17),CN t(16),H· · ·O s(11)
		92		$C^{\alpha}C$ t(22),NH ob(19),NC^{α} t(19),H· · ·O s(13)
107W	88			NC^{α} t(36),$C^{\alpha}C$ t(26),H· · ·O s(15),CN t(10)
	92			NC^{α} t(26),$C^{\alpha}C$ t(25),CN t(23),H· · ·O s(13)
	93			H· · ·O s(25),NC^{α} t(21),$C^{\alpha}C$ t(20),CO· · ·H ib(11)
			80	NH ob(25),$NC^{\alpha}C$ d(17),Nh· · ·O ib(16),$C^{\alpha}C$ t(10)
			92	NH ob(54),$NC^{\alpha}C$ d(23),H· · ·O s(19)
		45		NH ob(27),$NC^{\alpha}C$ d(23),NH· · ·O ib(11)
		33		NH ob(51),$NC^{\alpha}C$ d(33),H· · ·O s(11)
		40		H· · ·O s(33),NH ob(28),$NC^{\alpha}C$ d(17),NC^{α} t(10)
			44	NH ob(47),$NC^{\alpha}C$ d(29),NC^{α} t(18),$C^{\alpha}C$ t(14),CN t(13),H· · ·O s(12)
			43	$C^{\alpha}C$ t(47),NC^{α} t(24),NH ob(22),$NC^{\alpha}C$ d(16),CN t(12)
			32	$C^{\alpha}C$ t(46),H· · ·O s(25)
			31	NC^{α} t(31),$C^{\alpha}C$ t(26),NH· · ·O ib(24),NH ob(10)

[a] S = strong, M = medium, W = weak, V = very, sh = shoulder, ∥ = parallel dichroism, ⊥ = perpendicular dichroism.

[b] In the A and E_1 blocks, the modes are grouped in three's. In each group, the first entry is for the 3_{10}-helix, the second for the α-helix, and the third for the α'-helix. In the E_2 block, only modes due to α- and α'-helices are listed; the first of the group is due to α and the second to α'.

[c] s = stretch, as = antisymmetric stretch, ss = symmetric stretch, b = angle bend, ib = in-plane angle bend, ob = out-of-plane angle bend, ab = antisymmetric angle bend, sb = symmetric angle bend, r = rock, d = deformation, t = torsion, tw = twist. Only contributions of 10% or greater are included. Numbers 1 and 2 have been used in parentheses to distinguish the two methyl groups.

[d] Unperturbed frequency.

TABLE IV
Observed and Calculated Frequencies (in cm $^{-1}$) of N-Deuterated Poly(α-Aminoisobutyric Acid)

Observed[a]		Calculated[b]			
Raman	IR	A	E_1	E_2	Potential-Energy Distribution[c]
2988S	2986S$_\parallel$	2986			CH_3(1) as2(50),CH_3(2) as1(35),CH_3(2) as2(14)
		2985			CH_3(2) as1(47),CH_3(1) as2(46)
		2986			CH_3(1) as2(49),CH_3(2) as1(35),CH_3(2) as2(14)
2998M,sh	2998M,sh$_\perp$		2986		CH_3(1) as2(50),CH_3(2) as1(35),CH_3(2) as2(14)
			2985		CH_3(2) as1(46),CH_3(1) as2(46)
			2986		CH_3(1) as2(50),CH_3(2) as1(35),CH_3(2) as2(14)
				2985	CH_3(2) as1(47),CH_3(1) as2(46)
				2986	CH_3(1) as2(50),CH_3(2) as1(35),CH_3(2) as2(14)
2988S	2986S$_\parallel$	2984			CH_3(1) as1(49),CH_3(2) as2(35),CH_3(2) as1(15)
		2984			CH_3(2) as2(49),CH_3(1) as1(43)
		2984			CH_3(1) as1(47),CH_3(2) as2(37),CH_3(2) as1(15)
2998M,sh	2998M,sh$_\perp$		2984		CH_3(1) as1(53),CH_3(2) as2(33),CH_3(2) as1(14)
			2984		CH_3(1) as1(49),CH_3(2) as2(44)
			2984		CH_3(1) as1(48),CH_3(2) as2(37),CH_3(2) as1(14)
				2984	CH_3(2) as2(48),CH_3(1) as1(44)
				2984	CH_3(1) as1(48),CH_3(2) as2(37),CH_3(2) as1(15)
2988S	2986S$_\parallel$	2984			CH_3(1) as1(50),CH_3(2) as1(38),CH_3(2) as1(11)
		2984			CH_3(1) as1(51),CH_3(2) as2(30),CH_3(2) as1(18)
		2984			CH_3(1) as1(52),CH_3(2) as2(36),CH_3(2) as1(11)

2998M,sh	2998M,sh$_\perp$		2984		CH_3(1) as1(46),CH_3(2) as2(41),CH_3(2) as1(12)
			2984		CH_3(1) as1(46),CH_3(2) as2(34),CH_3(2) as1(19)
			2983		CH_3(1) as1(51),CH_3(2) as2(37),CH_3(2) as1(11)
				2984	CH_3(1) as1(50),CH_3(2) as1(31),CH_3(2) as1(18)
				2984	CH_3(1) as1(51),CH_3(2) as2(37),CH_3(2) as1(11)
2988S	2986S$_\parallel$	2982			CH_3(1) as2(50),CH_3(2) as1(38),CH_3(2) as2(12)
		2982			CH_3(1) as2(49),CH_3(2) as1(32),CH_3(2) as2(18)
		2982			CH_3(1) as2(50),CH_3(2) as1(38),CH_3(2) as2(12)
2998M,sh	2998M,sh$_\perp$		2982		CH_3(1) as2(49),CH_3(2) as1(38),CH_3(2) as2(12)
			2982		CH_3(1) as2(49),CH_3(2) as1(32),CH_3(2) as2(18)
			2982		CH_3(1) as2(49),CH_3(2) as1(38),CH_3(2) as2(12)
				2982	CH_3(1) as2(49),CH_3(2) as1(32),CH_3(2) as2(18)
				2982	CH_3(1) as2(50),CH_3(2) as1(38),CH_3(2) as2(12)
		2929			CH_3(1) ss(53),CH_3(2) ss(46)
		2929			CH_3(1) ss(65),CH_3(2) ss(35)
		2929			CH_3(2) ss(68),CH_3(1) ss(31)
2942VS			2929		CH_3(2) ss(61),CH_3(2) ss(39)
2934M,sh	2936M$_\perp$		2929		CH_3(2) ss(67),CH_3(1) ss(33)
			2929		CH_3(2) ss(81),CH_3(1) ss(19)
				2929	CH_3(1) ss(56),CH_3(2) ss(43)
				2929	CH_3(2) ss(99)

(*continued*)

Table IV (*continued*)

Observed[a]		Calculated[b]			
Raman	IR	A	E_1	E_2	Potential-Energy Distribution[c]
		2929			$CH_3(2)$ ss(53),$CH_3(1)$ ss(46)
		2929			$CH_3(2)$ ss(65),$CH_3(1)$ ss(35)
		2929			$CH_3(1)$ ss(68),$CH_3(2)$ ss(31)
2942VS			2929		$CH_3(1)$ ss(61),$CH_3(2)$ ss(39)
2934M,sh	2936M$_\perp$		2929		$CH_3(1)$ ss(67),$CH_3(2)$ ss(33)
			2929		$CH_3(1)$ ss(81),$CH_3(2)$ ss(19)
				2929	$CH_3(2)$ ss(56),$CH_3(1)$ ss(43)
				2929	$CH_3(1)$ ss(99)
	2434S$_\parallel$[d]	2397			ND s(96)
		2396			ND s(96)
		2396			ND s(96)
			2397		ND s(96)
			2396		ND s(96)
			2396		ND s(96)
				2396	ND s(96)
				2396	ND s(96)
	1640VS$_\parallel$	1655			CO s(82),CN s(16)
		1649			CO s(83),CN s(15)
		1658			CO s(82),CN s(17)
1640S			1655		CO s(82),CN s(15)
			1649		CO s(83),CN s(14),C^{a}CN d(10)
			1659		CO s(82),CN s(16)

				1641	CO s(82),CN s(14),C$^{\alpha}$CN d(10)
				1643	CO s(81),CN s(16)
	1472M$_{\downarrow}$		1484		CN s(29),C$^{\alpha}$C s(22),CO ib(14)
			1484		CN s(30),C$^{\alpha}$C s(21),CO ib(15)
			1481		CN s(27),C$^{\alpha}$C s(21),CO ib(14)
		1478			CN s(25),C$^{\alpha}$C s(17),CO ib(14),CH$_3$(2) ab1(12)
		1478			CN s(26),C$^{\alpha}$C s(17),CO ib(15),CH$_3$(2) ab1(12)
		1473			CN s(23),C$^{\alpha}$C s(17),CH$_3$ (2) ab1(16),CO ib(13)
				1488	CN s(32),C$^{\alpha}$C s(23),CO ib(14),NC$^{\alpha}$ s(10)
				1490	CN s(29),C$^{\alpha}$C s(23),CO ib(14),NC$^{\alpha}$ s(12)
1456S,sh	1468M$_{\downarrow}$	1456			CH$_3$(2) ab2(40),CH$_3$(1) ab1(37)
		1456			CH$_3$(1) ab1(41),CH$_3$(2) ab2(37)
		1456			CH$_3$(1) ab1(43),CH$_3$(2) ab2(37)
			1456		CH$_3$(1) ab1(30),CH$_3$(2) ab1(28),CH$_3$(2) ab2(14),CH$_3$(1) ab2(10)
			1457		CH$_3$(1) ab1(32),CH$_3$(2) ab1(25),CH$_3$(2) ab2(17)
			1456		CH$_3$(1) ab1(29),CH$_3$(2) ab1(28),CH$_3$(2) ab2(15), CH$_3$(1) ab2(10)
				1457	CH$_3$(2) ab1(37),CH$_3$(1) ab1(26),CH$_3$(1) ab2(11)
				1456	CH$_3$(2) ab1(43),CH$_3$(1) ab1(21),CH$_3$(1) ab2(15)
	1450W$_{\downarrow}$		1451		CH$_3$(1) ab2(45),CH$_3$(2) ab1(34)
			1450		CH$_3$(1) ab2(48),CH$_3$(2) ab1(28),CH$_3$(1) ab1(10)
			1451		CH$_3$(1) ab2(54),CH$_3$(2) ab1(25)
1452VS		1450			CH$_3$(1) ab2(43),CH$_3$(2) ab1(30),CH$_3$(1) ab1(14)
		1450			CH$_3$(1) ab2(45),CH$_3$(2) ab1(24),CH$_3$(1) ab1(18)
		1451			CH$_3$(1) ab2(54),CH$_3$(2) ab1(21),CH$_3$(1) ab1(11)

(*continued*)

Table IV (*continued*)

Observed[a]		Calculated[b]			
Raman	IR	A	E_1	E_2	Potential-Energy Distribution[c]
				1451	CH_3(1) ab2(50),CH_3(2) ab1(30)
				1451	CH_3(1) ab2(54),CH_3(2) ab1(28)
1452VS		1449			CH_3(2) ab2(48),CH_3(1) ab1(35)
		1449			CH_3(2) ab2(49),CH_3(1) ab1(28),CH_3(1) ab2(10)
		1449			CH_3(2) ab2(50),CH_3(1) ab1(33)
	1450W$_\perp$		1449		CH_3(2) ab2(42),CH_3(1) ab1(39)
			1449		CH_3(2) ab2(42),CH_3(1) ab1(36),CH_3(1) ab2(11)
			1449		CH_3(2) ab2(46),CH_3(1) ab1(37)
				1449	CH_3(1) ab1(40),CH_3(2) ab2(37),CH_3(1) ab2(13)
				1449	CH_3(1) ab1(41),CH_3(2) ab2(41)
	1424VS$_\perp$		1445		CH_3(2) ab2(28),CH_3(2) ab1(20),CH_3(1) ab2(17)
			1445		CH_3(2) ab1(28),CH_3(2) ab2(24),CH_3(1) ab2(15)
			1444		CH_3(2) ab1(28),CH_3(2) ab2(22),CH_3(1) ab1(12),CH_3(1) ab2(11)
		1443			CH_3(2) ab1(44),CH_3(1) ab2(24),CN s(12)
		1443			CH_3(2) ab1(46),CH_3(1) ab2(22),CN s(12)
		1442			CH_3(2) ab1(46),CH_3(1) ab2(17),CN s(14)
				1446	CH_3(2) ab2(40),CH_3(2) ab1(16),CH_3(1) ab1(12) CH_3(1) ab2(10)
				1446	CH_3(2) ab2(39),CH_3(1) ab1(20),CH_3(2) ab1(13)
	1384S$_\perp$		1385		CH_3(2) sb(47),CH_3(1) sb(38)
			1385		CH_3(2) sb(48),CH_3(1) sb(37)
			1386		CH_3(2) sb(46),CH_3(1) sb(35)

1374W	1377M$_{\parallel}$	1384			CH_3(2) sb(47),CH_3(1) sb(40)
		1385			CH_3(2) sb(47),CH_3(1) sb(39)
		1387			CH_3(2) sb(47),CH_3(1) sb(35)
				1384	CH_3(2) sb(49),CH_3(1) sb(35)
				1386	CH_3(2) sb(46),CH_3(1) sb(35)
	1363S$_{\perp}$		1365		CH_3(1) sb(55),CH_3(2) sb(47)
			1365		CH_3(1) sb(55),CH_3(2) sb(46)
			1365		CH_3(1) sb(56),CH_3(2) sb(47)
	1360M$_{\parallel}$	1363			CH_3(1) sb(56),CH_3(2) sb(48)
		1363			CH_3(1) sb(56),CH_3(2) sb(48)
		1363			CH_3(1) sb(58),CH_3(2) sb(46)
				1366	CH_3(1) sb(55),CH_3(2) sb(45)
				1366	CH_3(1) sb(55),CH_3(2) sb(47)
	1298W$_{\perp}$		1308		NC^{α} s(26),CC_2 ss(22),CH_3(2) r2(10)
			1307		NC^{α} s(26),CC_2 ss(21),CH_3(2) r2(10)
			1301		NC^{α} s(26),CC_2 ss(18),CH_3(2) r2(10)
		1292			NC^{α} s(30),CC_2 w(15),$C^{\alpha}C$ s(11)
		1300			NC^{α} s(32),CC_2 w(15)
		1299			NC^{α} s(33),CC_2 w(14)
				1308	CC_2 ss(25),NC^{α} s(24),CH_3(2) r2(11)
				1298	CC_2 ss(24),NC^{α} s(21),CH_3(2) r2(12)
	1233S$_{\perp}$		1246		CC_2 as(73),CC_2 r(14),CH_3(2) sb(13)
			1245		CC_2 as(73),CC_2 r(14),CH_3(2) sb(13)
			1253		CC_2 as(76),CH_3(2) sb(15),CC_2 r(13)

(*continued*)

Table IV (*continued*)

Observed[a]		Calculated[b]			
Raman	IR	A	E_1	E_2	Potential-Energy Distribution[c]
1229M		1235			CC_2 as(86),CC_2 r(17),CH_3(2) sb(11),CH_3(1) sb(10)
		1241			CC_2 as(82),CC_2 r(16),CH_3(1) sb(11),CH_3(2) sb(11)
		1251			CC_2 as(81),CC_2 r(15),CH_3(2) sb(13),CH_3(1) sb(12)
				1248	CC_2 as(70),CH_3(2) sb(14),CC_2 r(13),CH_3(1) r1(10)
				1254	CC_2 as(71),CH_3(2) sb(15),CC_2 r(12),CH_3(1) r1(10)
	1210S$_{\parallel}$	1217			CC_2 ss(20),CH_3(2) r1(15),CH_3(1) r1(14)
		1216			CC_2 ss(21),CH_3(1) r1(16),CH_3(2) r1(14),C$^{\alpha}$C s(11)
		1216			CC_2 ss(19),CH_3(1) r1(17),CH_3(2) r1(14),C$^{\alpha}$C s(11)
			1200		CH_3(2) r1(22),CC_2 as(13),CC_2 w(13),CH_3(1) r2(12)
			1200		CH_3(2) r1(21),CC_2 w(11),CH_3(1) r2(11)
			1201		CH_3(2) r1(19),CC_2 w(11),CH_3(1) r2(11),CC_2 ss(10)
				1193	CH_3(2) r1(25),CC_2 w(15),CH_3(1) r2(15),CC_2 as(11)
				1189	CH_3(2) r1(25),CH_3(1) r2(17),CC_2 w(15),CN s(11)
			1023		CH_3(1) r2(48),CH_3(2) r1(30),CH_3(2) r2(11)
			1023		CH_3(1) r2(48),CH_3(2) r1(31),CH_3(2) r2(11)
			1022		CH_3(1) r2(47),CH_3(2) r1(32),CH_3(2) r2(11)
1022M	1021W$_{\perp}$	1022			CH_3(1) r2(46),CH_3(2) r1(32),CH_3(2) r2(11)
		1023			CH_3(1) r2(47),CH_3(2) r1(32),CH_3(2) r2(11)
		1022			CH_3(1) r2(47),CH_3(2) r1(32),CH_3(2) r2(11)
				1023	CH_3(1) r2(48),CH_3(2) r1(30),CH_3(2) r2(11)
				1023	CH_3(1) r2(48),CH_3(2) r1(31),CH_3(2) r2(11)

			1007		CH_3(1) r1(36),ND ib(35)
			1001		CH_3(1) r1(40),CH_3(2) r2(20),ND ib(12),CH_3(2) r1(10)
			1005		CH_3(1) r1(35),CH_3(2) r2(20),ND ib(17),CH_3(2) r1(11)
1009W,sh	1014W$_\parallel$	1004			ND ib(28),CH_3(1) r1(23),CH_3(2) r1(16),CH_3(2) r2(14)
		1001			CH_3(1) r1(32),CH_3(2) r2(22),CH_3(2) r1(17),ND ib(11)
		1005			CH_3(1) r1(25),ND ib(19),CH_3(2) r1(19),CH_3(2) r2(19)
				1002	CH_3(1) r1(50),CH_3(2) r2(17),ND ib(12)
				1005	CH_3(1) r1(48),CH_3(2) r2(19),ND ib(14)
			996		CH_3(2) r2(36),ND ib(15),CC_2 as(13),CH_3(2) r1(12)
			986		CH_3(2) r2(27),ND ib(22),NC^α s(11)
			989		ND ib(34),CH_3(2) r2(19)
980W	983VW$_\parallel$	991			ND ib(34),CH_3(2) r2(17),CH_3(1) r1(15),CC_2 as(14)
		978			ND ib(39),CH_3(2) r2(13),NC^α s(10),CH_3(1) r2(10)
		988			ND ib(37),CH_3(1) r1(15),CC_2 as(11),CH_3(2) r2(11)
				991	CH_3(2) r2(36),ND ib(16),NC^α s(11),CC_2 ss(10)
				991	CH_3(2) r2(30),ND ib(26),CH_3(2) r1(11),NC^α s(10)
			966		CC_2 ss(18),ND ib(18),CH_3(1) r1(18),CH_3(2) r2(14)
			960		ND ib(33),CC_2 ss(18),CH_3(1) r1(15),CH_3(2) r2(10)
			962		CC_2 ss(21),CH_3(1) r1(17),ND ib(16),CH_3(2) r2(16)
943VS	941W$_\parallel$	953			CC_2 ss(30),CH_3(2) r2(22),CH_3(1) r1(15),NC^α s(12)
		959			CC_2 ss(35),CH_3(1) r1(21),CH_3(2) r2(21)
		959			CC_2 ss(25),CH_3(2) r2(24),CH_3(1) r1(14),NC^α s(13) CH_3(1) r2(11)
				959	ND ib(46),CC_2 ss(11),CH_3(1) r1(11)
				960	ND ib(34),CC_2 ss(15),CH_3(1) r1(15)

(*continued*)

Table IV (*continued*)

Observed[a]		Calculated[b]			
Raman	IR	A	E_1	E_2	Potential-Energy Distribution[c]
	942W$_\perp$		926		CN s(19),CH_3(2) r1(11),CNC$^\alpha$ d(10),CH_3(1) r2(10)
			924		CN s(19),CH_3(2) r1(10)
			922		CN s(18),CH_3(2) r1(10)
917M	917W$_\parallel$	918			CC_2 ss(23),C$^\alpha$C s(17),CN s(13),CH_3(2) r1(12)
		913			CN s(18),C$^\alpha$C s(14),CC_2 ss(10),ND ib(10)
		920			CC_2 ss(22),CN s(17),C$^\alpha$C s(16)
				929	CN s(20),CH_3(2) r1(11),CNC$^\alpha$ d(10),CH_3(1) r2(10)
				926	CN s(19),CH_3(2) r1(12),CH_3(1) r2(11),CNC$^\alpha$ d(10)
891VS	886VW$_\parallel$	879			CNC$^\alpha$ d(21),CO ib(13),CN s(11)
		874			CNC$^\alpha$ d(17),ND ib(15),CC_2 ss(12),CO ib(12)
		868			ND ib(18),CNC$^\alpha$ d(16),CO ib(12),CC_2 ss(12)
821M	822W$_\perp$		823		CC_2 ss(44),NC$^\alpha$ s(18),CO ib(12)
			834		CC_2 ss(31),NC$^\alpha$ s(15),CO ib(12)
			840		CC_2 ss(26),NC$^\alpha$ s(15),CO ib(12)
				809	CC_2 ss(52),NC$^\alpha$ s(13),CO ob(11)
				810	CC_2 ss(48),CO ob(25)
	770W$_\perp$		772		CO ob(58)
			770		CO ob(54),CC_2 ss(10)
			775		CO ob(50),CC_2 ss(14)
762M		749			CO ob(66),CC_2 r(10)
		739			CO ob(64)
		740			CO ob(58)

				777	CO ob(45),NC$^{\alpha}$ s(12)
				792	CO ob(29),NC$^{\alpha}$ s(25)
640M			639		C$^{\alpha}$C s(20),CC$_2$ w(17),CO ib(14),C$^{\alpha}$CN d(10)
			625		CC$_2$ w(21),C$^{\alpha}$C s(16),CO ib(16),C$^{\alpha}$CN d(10)
			612		CC$_2$ w(18),CO ib(17)C$^{\alpha}$C s(16),C$^{\alpha}$CN d(12)
583M	585M$_{\parallel}$	611			NC$^{\alpha}$C d(18),CC$_2$ ss(16),ND ob(11)
		593			NC$^{\alpha}$C d(19),CC$_2$ ss(13)
		599			NC$^{\alpha}$C d(16),CC$_2$ ss(12)
				665	C$^{\alpha}$C s(21),CC$_2$ w(21),CO ib(14)
				668	C$^{\alpha}$C s(22),CC$_2$ w(19),CO ib(12)
568VS		562			CC$_2$ w(24),C$^{\alpha}$CN d(20),CO ib(19),NC$^{\alpha}$ s(15)
		564			C$^{\alpha}$CN d(30),CC$_2$ w(16),CO ib(14),CC$_2$ r(14)
		568			C$^{\alpha}$CN d(29),CC$_2$ r(19)
	526M,sh$_{\perp}$		536		ND ob(30),CN t(30),CC$_2$ r(14)
			514		ND ob(27),CN t(25),CC$_2$ r(16),NC$^{\alpha}$C d(12)
			519		CC$_2$ r(20),ND ob(19),CN t(15),NC$^{\alpha}$C d(11)
				500	CN t(66),ND ob(38),ND· · ·O ib(11)
				482	CN t(61),ND ob(37)
		497			CN t(53),ND ob(32),CC$_2$ w(12),C$^{\alpha}$CN d(12),ND· · ·O ib(10)
		476			CN t(64),ND ob(42),CC$_2$ w(12),ND· · ·O ib(11),CC$_2$ b(11)
		459			CN t(45),ND ob(33),CC$_2$ w(18),CC$_2$ b(16)
	508M$_{\perp}$		485		CN t(44),CC$_2$ r(28)
			477		CN t(46),CC$_2$ r(21)
			479		CN t(27),CC$_2$ r(15),CC$_2$ b(12)

(*continued*)

Table IV (*continued*)

Observed[a]		Calculated[b]			
Raman	IR	A	E_1	E_2	Potential-Energy Distribution[c]
				472	CC_2 r(26),CO ib(19),$C^{\alpha}C$ s(10),CN t(10)
				476	CO ib(27),CC_2 r(22),$C^{\alpha}C$ s(10)
429M	428$M_{\perp}$		428		CC_2 b(53),CO ib(12)
			432		CC_2 b(45),CN t(21),ND ob(20)
			427		CN t(51),ND ob(32),CC_2 b(26)
416W		418			CC_2 tw(31),CN t(22),CC_2 b(16)
		407			CN t(27),CC_2 b(23),CC_2 tw(15)
		396			CN t(50),CC_2 b(23),ND ob(19),CO ob(11)
				408	CC_2 b(60),CN t(12),ND ob(11)
				416	CC_2 b(31),CC_2 tw(24),CN t(13),$C^{\alpha}CN$ d(10)
374W	372$M_{\perp}$		360		CC_2 w(20),CC_2 tw(16),$C^{\alpha}CN$ d(14),CC_2 b(13),CO ib(10)
			350		CO ib(18),CC_2 w(18),CC_2 tw(14),CC_2 b(11)
			355		CC_2 b(21),CC_2 w(16),CC_2 tw(13),CN t(10)
364M	365$M_{\parallel}$	350			CC_2 w(33),CC_2 b(15)
		363			CC_2 w(23),CC_2 b(21),CC_2 r(11),CO ob(11)
		365			CC_2 w(33),CC_2 b(17),CO ob(10)
				372	CC_2 tw(34),CC_2 b(20),$C^{\alpha}CN$ d(14)
				378	CC_2 b(40),CC_2 tw(22),CN t(12)
		330			CO ib(29),CC_2 r(24),CNC^{α} d(11)
		337			CO ib(38),$C^{\alpha}C$ s(14),CC_2 r(13),CC_2 w(12)
		322			CO ib(36),CC_2 r(16),$C^{\alpha}C$ s(13)

317M	$319M_{\perp}$		321		CC_2 tw(26),CO ib(13),CC_2 b(12),$NC^{\alpha}C$ d(10),CNC^{α} d(10)
			321		CC_2 tw(25),CC_2 b(18),$NC^{\alpha}C$ d(10),CO ib(10)
			314		CO ib(20),CC_2 tw(17),CC_2 b(16),$NC^{\alpha}C$ d(12),CNC^{α} d(10)
				315	CC_2 w(21),CO ib(17),CC_2 r(11)
				307	CC_2 w(22),CC_2 r(18),CO ib(14)
299S		289			CC_2 b(36),CC_2 tw(30)
		283			CC_2 tw(44),CC_2 b(29)
		279			CC_2 tw(48),CC_2 (25)
281S			274		CC_2 w(18),CC_2 tw(17),CC_2 b(11),CC_2 r(11),CO ob(11)
			288		CC_2 tw(28),CC_2 w(20),CC_2 b(13),CC_2 r(10)
			289		CC_2 tw(34),CC_2 w(20),CC_2 b(11),CC_2 r(10)
				262	CC_2 tw(16),CO ob(15),CC_2 w(13),$NC^{\alpha}C$ d(13)
				269	CC_2 w(19),$NC^{\alpha}C$ d(14),CO ob(11),CNC^{α} d(10)
226VW		223			$C^{\alpha}C^{\beta}$ t(95)
		223			$C^{\alpha}C^{\beta}$ t(84)
		221			$C^{\alpha}C^{\beta}$ t(94)
			223		$C^{\alpha}C^{\beta}$ t(93)
			224		$C^{\alpha}C^{\beta}$ t(93)
			224		$C^{\alpha}C^{\beta}$ t(94)
				223	$C^{\alpha}C^{\beta}$ t(89)
				223	$C^{\alpha}C^{\beta}$ t(89)
215W		220			$C^{\alpha}C^{\beta}$ t(97)
		219			$C^{\alpha}C^{\beta}$ t(97)
		219			$C^{\alpha}C^{\beta}$ t(97)

(*continued*)

Table IV (*continued*)

Observed[a]		Calculated[b]			
Raman	IR	A	E_1	E_2	Potential-Energy Distribution[c]
			218		$C^{\alpha}C^{\beta}$ t(97)
			218		$C^{\alpha}C^{\beta}$ t(97)
			218		$C^{\alpha}C^{\beta}$ t(97)
				219	$C^{\alpha}C^{\beta}$ t(95)
				220	$C^{\alpha}C^{\beta}$ t(95)
189M			186		$C^{\alpha}CN$ d(28),CC_2 tw(11)
			174		$C^{\alpha}CN$ d(29),CC_2 r(11)
			169		$C^{\alpha}CN$ d(23),CC_2 tw(10)
163M		164			$C^{\alpha}CN$ d(21),CC_2 tw(18)
		186			CC_2 tw(21),$C^{\alpha}CN$ d(17)
		179			CC_2 tw(18),$C^{\alpha}CN$ d(15),CNC^{α} d(11)
				196	$C^{\alpha}CN$ d(29),CC_2 tw(14),CC_2 w(11),CC_2 r(10)
				194	$C^{\alpha}CN$ d(35),CC_2 tw(20)
		136			CNC^{α} d(38),CC_2 r(16),$C^{\alpha}CN$ d(13),D · · · O s(10)
		115			CNC^{α} d(39),CC_2 r(24),$C^{\alpha}CN$ d(20)
		112			CNC^{α} d(33),CC_2 r(28),$C^{\alpha}CN$ d(25)
116M					
			120		CNC^{α} d(30),ND ob(22)
			131		CNC^{α} d(39),CC_2 r(13),ND ob(12)
			136		CNC^{α} d(29),CC_2 r(22),D · · · O s(15),$C^{\alpha}CN$ d(12)

			121	CNC^{α} d(30),ND ob(23),CC_2 r(12)
			137	CNC^{α} d(25),CC_2 r(15),D · · · O s(10),CO ob(10)
107W		92		D · · · O s(20),$C^{\alpha}C$ t(17),ND ob(15),NC^{α} t(13),CN t(10)
		87		$C^{\alpha}C$ t(21),ND ob(18),NC^{α} t(17),CN t(15),D · · · O s(10)
		91		$C^{\alpha}C$ t(22),ND ob(19),NC^{α} t(19),D · · · O s(13)
	87			NC^{α} t(36),$C^{\alpha}C$ t(26),D · · · O s(15),CN t(10)
	92			NC^{α} t(26),$C^{\alpha}C$ t(25),CN t(22),D · · · O s(13)
	92			D · · · O s(92),NC^{α} t(21),$C^{\alpha}C$ t(20),CO · · · D ib(11)
			80	ND ob(25),$NC^{\alpha}C$ d(17),ND · · · O ib(17),NC^{α} t(10),$C^{\alpha}C$ t(10)
			92	ND ob(54),$NC^{\alpha}C$ d(24),D · · · O s(20)
		45		ND ob(27),$NC^{\alpha}C$ d(23),ND · · · O ib(11)
		33		ND ob(51),$NC^{\alpha}C$ d(32),D · · · O s(11)
		40		D · · · O s(33),ND ob(28),$NC^{\alpha}C$ d(17),NC^{α} t(10)
			43	ND ob(47),$NC^{\alpha}C$ d(26),NC^{α} t(19),$C^{\alpha}C$ t(14),CN t(13),D · · · O s(13)
			43	$C^{\alpha}C$ t(46),NC^{α} t(25),ND ob(22),$NC^{\alpha}C$ d(16),CN t(11)
			31	$C^{\alpha}C$ t(47),D · · · O s(25)
			31	NC^{α} t(30),$C^{\alpha}C$ t(27),ND · · · O ib(24)

[a] S = strong, M = medium, W = weak, V = very, sh = shoulder, ∥ = parallel dichroism, ⊥ = perpendicular dichroism.

[b] In the A and E_1 blocks the modes are grouped in three's. In each group, the first entry is for the 3_{10}-helix, the second for the α-helix, and the third for the α'-helix. In the E_2 block, only modes due to α- and α'-helices are listed; the first of the group is due to α and the second to α'.

[c] s = stretch, as = antisymmetric stretch, ss = symmetric stretch, b = angle bend, ib = in-plane angle bend, ob = out-of-plane angle bend, ab = antisymmetric angle bend, sb = symmetric angle bend, r = rock, d = deformation, t = torsion, tw = twist. Only contributions of 10% or greater are included. Numbers 1 and 2 have been used in parentheses to distinguish the two methyl groups.

[d] Unperturbed frequency.

$\nu_A^0 \cong 3260$ cm^{-1} is now seen to be intermediate between those for α-(3279 cm^{-1}) and β-poly(L-alanine) (3242 cm^{-1}).[34] This indicates that the hydrogen bond in PAIB is stronger than that in an α-helix, which would be consistent with the proposed 3_{10}-helix structure (and, incidentally, inconsistent with the α'-helix structure—see Table I). Our adjustment of f(CO), f(NH), and f(H $\cdots$ O) (see above) is reasonably based on this observation and leads to a good prediction of this frequency. [It is important to note that the predicted frequencies of ν_A^0 for the α- and α'-helices are essentially the same as for the 3_{10}-helix because we have, inappropriately, kept these force constants the same for all three structures; this was done in order to examine only the effects of conformational differences. Appropriate values of these force constants would result in a higher predicted frequency for the α-helix ($\sim$3279 cm^{-1}) and a much higher frequency for the α'-helix.]

The ν_B^0 values also support a 3_{10}-helix structure. If, as is likely,[34] these two bands arise from overtones of amide II, then their observed difference of 27 cm^{-1} is more consistent with the predicted (and calculated) difference of 28 cm^{-1} for the 3_{10}-helix ($2 \times 1545 - 2 \times 1531 = 3090 - 3062 = 28$) than with the expected difference of 42 cm^{-1} for the other structures. Interestingly, both ν_B^0 values are about 20 cm^{-1} lower than the expected values of the overtones for the 3_{10}-helix, whereas for α-poly(L-alanine), the difference is 4 cm^{-1}.[34] This may indicate that the anharmonicities in PAIB are significantly different from those in an α-helix, thus providing further evidence that the structure is not α-helical. Such a difference could arise from the greater crowding of backbone atoms in the 3_{10}-helix than in the α-helix: $C^\alpha \cdots O$, $N \cdots N$, and $N \cdots O$ distances are significantly shorter in the former than in the latter structure.

The CH_3 stretch modes are reasonably well accounted for, although we do not reproduce small splittings in the ir bands nor between ir and Raman. As in a similar situation in α-poly(L-alanine),[18,21] such splittings may arise from intermolecular $CH_3 \cdots CH_3$ interactions.

The observed difference between Raman and ir amide I (mainly CO stretch) modes is 3 cm^{-1} in α-poly(L-alanine)[18] and 9 cm^{-1} in PAIB. The predicted difference for the 3_{10}-helix is 4 cm^{-1}, but this is twice as large as that predicted for the α-helix (with no difference predicted for the α'-helix). As noted above, these splittings are contributed to by transition dipole coupling interactions and reflect the conformational differences between the helices. The absolute frequency agreement cannot be compared because of the use of the same f(CO) force constant for all three structures. If this force constant were adjusted in accordance with the relative hydrogen-bond strengths, then, as discussed above, a higher frequency would be calculated for the α-helix and a much higher frequency for the α'-helix.

The amide II modes (NH in-plane bend plus CN stretch) are very well predicted by the 3_{10}-helix, whereas the α- and α'-helices give sig-

nificantly lower frequencies than are observed. This must be predominantly a conformational effect, since the relevant force constants are the same for all structures.

The CH_3 bend modes are, of course, predicted comparably by all three structures. The frequency agreement is satisfactory, except that the splitting between the $1455_{\perp}$ and $1467_{\parallel}$ cm^{-1} bands in the ir is not accounted for by the calculation, probably for reasons similar to those discussed in connection with the CH_3 stretch modes.

In the 1350–1200-cm^{-1} region, we find bands associated with CC_2 stretch and with amide III (mostly NH in-plane bend) modes. Although the frequency agreement is reasonable for all the structures, the predictions for the 3_{10}-helix are somewhat better, as is seen for bands near 1303, 1280, and 1212 cm^{-1}. It is gratifying, if not surprising, that the calculation accounts well for strong ir bands at $1227_{\perp}$ and $1210_{\parallel}$ cm^{-1} associated with CC_2 stretch, in a region where no absorption is found for α-poly(L-alanine).[18,21]

In the 1200–700-cm^{-1} region, most modes allow no real distinction to be made between the three structures. (We have no explanation for the Raman bands observed in the 1125–1040-cm^{-1} region: none of the structures predicts such vibrational modes. The intensity level in this region varies from sample to sample and seems to be related to the fluorescence of the sample.) The observed bands near 820M cm^{-1} distinctly favor the 3_{10}-helix (although this is countered by the poorer agreement for the 762W Raman band).

In the conformation-sensitive region below 700 cm^{-1}, several observed bands strongly favor the 3_{10}-helix. Thus, the amide V (NH out-of-plane bend plus CN torsion) modes at $694S_{\perp}$ and $680M_{\parallel}$ cm^{-1} in the ir are very well accounted for by the 3_{10}-helix, but very large discrepancies occur for the α- and α'-helices. A Raman band at 642W cm^{-1} is satisfactorily predicted by the 3_{10}-helix structure but not as well by the others. The observed bands near 425 cm^{-1} are best accounted for by the 3_{10}-helix. And the correct order of the $367M_{\perp}$ and $362S_{\parallel}$ CC_2 wag modes is given only by the 3_{10}-helix.

In summary, several key features in the comparison between observed and calculated frequencies of PAIB definitively favor a predominant 3_{10}-helix conformation of this polypeptide in monolayer films. The α'-helix is clearly disfavored.

Poly(α-Aminoisobutyric Acid)-ND

The results of N-deuteration are consistent with the normal mode calculation on PAIB. They also favor, although not as conclusively, the 3_{10}-helix.

The ND stretch modes are found at 2414S and 2460M cm^{-1} in the ir. In distinction to α-poly(L-alanine),[34] the fundamental contributes mostly to the lower frequency. Also, no splitting is observed in amide

B′, which was the case for PAIB. From the observed integrated area ratio $I_{B'}/I_{A'} = 0.794$, we find $\nu^0_{A'} = 2434$ and $\nu^0_{B'} = 2440$ cm^{-1}. The calculated ND stretch frequency, using the same value of f(NH) as in PAIB, is 37 cm^{-1} lower than $\nu^0_{A'}$. This is similar to the situation for α- and β-poly(L-alanine-ND),[34] where differences of 40–50-cm^{-1} occur, and is probably due to different anharmonicities in PAIB and PAIB-ND. If $\nu^0_{B'}$ is associated with a combination similar to that found in poly(L-alanine-ND),[34] namely, between amide II′ (mainly CN plus C$^{\alpha}$C stretch) and ND in-plane bend, then a possibility is 1472(E_1) + 966(E_1) = 2438(A). The specific combination may be uncertain because of lack of information about anharmonicities.

The CO stretch mode is found to shift down by 16 cm^{-1} in the ir, from 1656 to 1640 cm^{-1}, significantly more than the 8 cm^{-1} observed in α-poly(L-alanine).[18,21] (We attribute the observed ir bands near 1655 and 1650 cm^{-1} to the presence of a significant amount of undeuterated material.) The calculated decreases are 10, 8, and 7 cm^{-1} for the 3_{10}-, α-, and α'-helices, respectively. The comparable Raman shift is 7 cm^{-1} compared to 3 cm^{-1} for α-poly(L-alanine). The calculated shift in this case is 6 cm^{-1}, the same for all three structures.

The appearance of the amide II′ mode at 1472 cm^{-1} is expected and reasonably well predicted. The CH_3 antisymmetric bend modes of PAIB near 1467(ir) and 1450(R) cm^{-1} are also observed in PAIB-ND, but what is surprising is that other CH_3 bend modes appear in the spectra of the deuterated molecule. This would seem to be the case for the surprisingly strong new band at 1424 cm^{-1} (which is not too well predicted) and a CH_3 symmetric bend mode near 1375 cm^{-1}. Assuming these assignments to be correct, such intensity changes may arise from a change in the local environment of the CH_3 groups.

The observed bands in PAIB having a significant NH in-plane bend component, viz., at 1339(R), 1313(R), and 1280(R,ir) cm^{-1}, disappear, as expected, on N-deuteration, which is well accounted for by the calculation on PAIB-ND. As a result, although some of the other modes in this general region (1350–1150 cm^{-1}) are predicted to remain essentially constant, and do (e.g., near 1230 and 1210 cm^{-1}), still others are expected to shift: the mode near 1300 cm^{-1} is predicted to shift up slightly, but is found to move about the same amount in the opposite direction; and the mode near 1170 cm^{-1} is predicted to shift up significantly and change in character, and the observed band in PAIB is absent in the spectra of PAIB-ND. It is difficult to choose between the structures on the basis of this region, although the small shift in the 1210(ir) cm^{-1} band and the frequency agreement for the 1229(R) cm^{-1} band would both tend to favor the 3_{10}-helix. Incidentally, the new bands in PAIB-ND near 1010 and 980 cm^{-1} due to ND in-plane bend are moderately well accounted for by the calculation, although they can provide no diagnostic help because of the uncertainties about anharmonicities.

In the 1000–500-cm^{-1} region, the skeletal stretch and deformation modes behave generally as predicted, with a tendency to favor the 3_{10}-helix. The 950(R) cm^{-1} band of PAIB is predicted to shift down by about 5 cm^{-1}, and is observed to do so. The predicted downward shift of the PAIB bands near 920 cm^{-1} is found, although a structural preference is not possible. The case of the 908(R) cm^{-1} band of PAIB is an interesting one. It is predicted to undergo a large shift in PAIB-ND, which is found, with this shift being in slightly better agreement with the 3_{10}-helix than the α-helix and in very poor agreement with the predictions of the α'-helix. As in PAIB, the bands near 820 cm^{-1} clearly favor the 3_{10}-helix, as is now true of the 762(R) cm^{-1} band and continues to be the case for the 640(R) cm^{-1} band. The 583(R) cm^{-1} band of PAIB is poorly reproduced by the 3_{10}-helix, but this may be due to the contribution of ND out-of-plane bend. A similar problem may exist with the 526(ir) cm^{-1} band. The calculation suggests that the character and frequency of the 505(ir) cm^{-1} band of PAIB should change significantly in PAIB-ND, but this is not apparent, and it is therefore difficult to use this band as an indicator of structure.

Below 500 cm^{-1}, N-deuteration does not produce many changes in PAIB-ND as compared to PAIB. It is interesting, however, that a calculated A-species mode near 430 cm^{-1} in PAIB, for which there was no observed counterpart, is predicted to shift down significantly in PAIB-ND, and the new observed 416(R) cm^{-1} band is in distinctly better agreement with the 3_{10}-helix.

CONCLUSIONS

The ir and Raman spectra of PAIB prepared as monomolecular films, when combined with normal mode calculations on 3_{10}, α-, and α'-helices, indicate strongly that the chain backbone has a 3_{10}-helix conformation. This is in agreement with conclusions reached from electron diffraction studies.[7,8]

It is not only that the average discrepancy between observed and calculated frequencies is significantly less for the 3_{10}-helix as compared to the other two helical structures, although this is the case: for observed bands below 1700 cm^{-1} the average observed discrepancy is 5.9 cm^{-1} for the 3_{10}-helix, 10.1 cm^{-1} for the α-helix, and 12.5 cm^{-1} for the α'-helix. (We note that a discrepancy of 5–6 cm^{-1} is typical of that found for the standard α-helix and β-sheet structures to which the force field was refined.[23]) More importantly, certain special features of the spectra are accounted for better by the 3_{10}-helix: the presence and observed splitting of the two ν_B^0 modes, where only one band is seen for the α-helix; the larger splitting between ir and Raman amide I modes than is predicted, or found, for α-helix structures; the significantly higher amide II frequency; and the significantly better agreement for the amide V mode. Other, more general, agreement with the 3_{10}-helix is evident throughout the spectral range.

These results demonstrate the power of normal mode analysis in permitting critical distinctions in conformation to be made from vibrational spectra.

We thank Dr. V. Sasisekharan for providing the coordinates of the 3_{10}-helix structure. This research was supported by NSF Grants PCM-8214064 and DMR-8303610.

References

1. Burgess, A. W. & Leach, S. J. (1973) *Biopolymers* **12**, 2599–2605.

2. Venkataram Prasad, B. V. & Sasisekharan, V. (1979) *Macromolecules* **12**, 1107–1110.

3. Paterson, Y., Rumsey, S. M., Benedetti, E., Némethy, G. & Scheraga, H. A. (1981) *J. Am. Chem. Soc.* **103**, 2947–2948.

4. Paterson, Y., Stimson, E. R., Evans, D. J., Leach, S. J. & Scheraga, H. A. (1982) *Int. J. Pept. Protein Res.* **20**, 468–480.

5. Benedetti, E., Bavoso, A., DiBlasio, B., Pavone, V., Pedone, C., Toniolo, C. & Bonora, G. M. (1982) *Proc. Natl. Acad. Sci. USA* **79**, 7951–7954.

6. Marshall, G. R. & Bosshard, H. E. (1972) *Circ. Res. Suppl. II* **30/31**, 143–150.

7. Malcolm, B. R. (1977) *Biopolymers* **16**, 2591–2592.

8. Malcolm, B. R. (1983) *Biopolymers* **22**, 319–321.

9. Shamala, N., Nagaraj, R. & Balaram, P. (1977) *Biochem. Biophys. Res. Commun.* **79**, 292–298.

10. Smith, G. D., Duax, W. L., Czerwinski, E. W., Kendrick, N. E., Marshall, G. R. & Matthews, F. S. (1977) *Peptides: Proceedings of the Fifth American Peptide Symposium*, Wiley, New York, pp. 277–279.

11. Shamala, N., Nagaraj, R. & Balaram, P. (1978) *J. Chem. Soc. Commun.*, 996–997.

12. Venkataram Prasad, B. V., Shamala, N., Nagaraj, R. & Balaram, P. (1980) *Acta Crystallogr., Sect. B* **36**, 107–110.

13. Nagaraj, R., Shamala, N. & Balaram, P. (1979) *J. Am. Chem. Soc.* **101**, 16–20.

14. Venkataram Prasad, B. V., Shamala, N., Nagaraj, R., Chandrasekaran, R. & Balaram, P. (1979) *Biopolymers* **18**, 1635–1646.

15. Smith, G. D., Pletnev, V. Z., Duax, W. L., Balasubramanian, T. M., Bosshard, H. E., Czerwinski, E. W., Kendrick, N. E., Matthews, F. S. & Marshall, G. R. (1981) *J. Am. Chem. Soc.* **103**, 1493–1501.

16. Moore, W. H. & Krimm, S. (1976) *Biopolymers* **15**, 2439–2464.

17. Moore, W. H. & Krimm, S. (1976) *Biopolymers* **15**, 2465–2483.

18. Rabolt, J. F., Moore, W. H. & Krimm, S. (1977) *Macromolecules* **10**, 1066–1074.

19. Dwivedi, A. M. & Krimm, S. (1982) *Macromolecules* **15**, 177–185.

20. Dwivedi, A. M. & Krimm, S. (1982) *Macromolecules* **15**, 186–193; (1983) **16**, 340.

21. Dwivedi, A. M. & Krimm, S. (1984) *Biopolymers* **23**, 923–943.

22. Dwivedi, A. M. & Krimm, S. (1984) *J. Phys. Chem.* **88**,620–627.

23. Krimm, S. (1983) *Biopolymers* **22**, 217–225.

24. Bandekar, J. & Krimm, S. (1979) *Proc. Natl. Acad. Sci. USA* **76**, 774–777.

25. Krimm, S. & Bandekar, J. (1980) *Biopolymers* **19**, 1–29.

26. Bandekar, J. & Krimm, S. (1980) *Biopolymers* **19**, 31–36.

27. Maxfield, F. R., Bandekar, J., Krimm, S., Evans, D. J., Leach, S. J., Némethy, G. & Scheraga, H. A. (1981) *Macromolecules* **14**, 997–1003.

28. Bandekar, J., Evans, D. J., Krimm, S., Leach, S. J., Lee, S., McQuie, J. R., Minasian, E., Némethy, G., Pottle, M. S., Scheraga, H. A., Stimson, E. R. & Woody, R. W. (1982) *Int. J. Pept. Protein Res.* **19**, 187–205.

29. Krimm, S. & Dwivedi, A. M. (1982) *Science* **216**, 407–408.

30. Dwivedi, A. M. & Krimm, S. (1982) *Biopolymers* **21**, 2377–2397.

31. Elliott, A. (1954) *Proc. R. Soc. London, Ser. A* **226**, 408–421.

32. Arnott, S. & Dover, S. D. (1967) *J. Mol. Biol.* **30**, 209–212.
33. Donohue, J. (1953) *Proc. Natl. Acad. Sci. USA* **39**, 470–478.
34. Krimm, S. & Dwivedi, A. M. (1982) *J. Raman Spectrosc.* **12**, 133–137.

Received December 12, 1983
Accepted April 9, 1984